PHILOSOPHICAL TRANSACTIONS OF THE ROYAL SOCIETY A MATHEMATICAL, PHYSICAL & ENGINEERING SCIENCES

Seismic Modelling of the Earth's Large-Scale Three-Dimensional Structure

J. H. Woodhouse and A. M. Dziewonski

Phil. Trans. R. Soc. Lond. A 1989 **328**, 291-308
doi: 10.1098/rsta.1989.0037

Phil. Trans. R. Soc. Lond. A **328**, 291–308 (1989)
Printed in Great Britain

Seismic modelling of the Earth's large-scale three-dimensional structure

By J. H. Woodhouse and A. M. Dziewonski

Department of Earth and Planetary Sciences, Harvard University, 20 Oxford Street, Cambridge, Massachusetts 02138, *U.S.A.*

[Plates 1 and 2]

Several different kinds of seismological data, spanning more than three orders of magnitude in frequency, have been employed in the study of the Earth's large-scale three-dimensional structure. These yield different but overlapping information, which is leading to a coherent picture of the Earth's internal heterogeneity. In this article we describe several methods of seismic inversion and intercompare the resulting models.

Models of upper-mantle shear velocity based upon mantle waveforms (Woodhouse & Dziewonski (*J. geophys. Res.* **89**, 5953–5986 (1984))) ($f \lesssim 7$ mHz) and long-period body waveforms ($f \lesssim 20$ mHz; Woodhouse & Dziewonski (*Eos, Wash.* **67**, 307 (1986))) show the mid-oceanic ridges to be the major low-velocity anomalies in the uppermost mantle, together with regions in the western Pacific, characterized by back-arc volcanism. High velocities are associated with the continents, and in particular with the continental shields, extending to depths in excess of 300 km. By assuming a given ratio between density and wave velocity variations, and a given mantle viscosity structure, such models have been successful in explaining some aspects of observed plate motion in terms of thermal convection in the mantle (Forte & Peltier (*J. geophys. Res.* **92**, 3645–3679 (1987))). An important qualitative conclusion from such analysis is that the magnitude of the observed seismic anomalies is of the order expected in a convecting system having the viscosity, temperature derivatives and flow rates which characterize the mantle.

Models of the lower mantle based upon P-wave arrival times ($f \approx 1$ Hz; Dziewonski (*J. geophys. Res.* **89**, 5929–5952 (1984)); Morelli & Dziewonski (*Eos, Wash.* **67**, 311 (1986))) SH waveforms ($f \approx 20$ mHz; Woodhouse & Dziewonski (1986)) and free oscillations (Giardini *et al.* (*Nature, Lond.* **325**, 405–411 (1987); *J. geophys. Res.* **93**, 13716–13742 (1988))) ($f \approx 0.5$–5 mHz) show a very long wavelength pattern, largely contained in spherical harmonics of degree 2, which is present over a large range of depths (1000–2700 km). This anomaly has been detected in both compressional and shear wave velocities, and yields a ratio of relative perturbations in v_S and v_P in the lower mantle in the range 2–2.5. Such values, which are much larger than has sometimes been assumed, roughly correspond to the case that perturbations in shear modulus dominate those in bulk modulus. It is this anomaly that is mainly responsible for the observed low-degree geoid undulations (Hager *et al.* *Nature, Lond.* **313**, 541–545 (1985))). In the upper part of the lower mantle this pattern consists of a high-velocity feature skirting the subduction zones of the Pacific and extending from Indonesia to the Mediterranean, with low velocities elsewhere; thus it appears to be associated with plate convergence and subduction. The pattern of wave speeds in the lowermost mantle is such that approximately 80% of hot spots are in regions of lower than average velocities in the D″ region.

The topography of the core–mantle boundary, determined from the arrival times of reflected and transmitted waves (Morelli & Dziewonski (*Nature, Lond.* **325**, 678–683 (1987))), exhibits a pattern of depressions encircling the Pacific, having an

amplitude of approximately ±5 km, which has been shown to be consistent with the stresses induced by density anomalies inferred from tomographic models of the lower mantle (Forte & Peltier (*Tectonophysics* (In the press.) (1989))).

By using both free oscillations (Woodhouse *et al.* (*Geophys. Res. Lett.* **13**, 1549–1552 (1986))) and travel-time data (Morelli *et al.* (*Geophys. Res. Lett.* **13**, 1545–1548 (1986))), the inner core has been found to be anisotropic, exhibiting high velocities for waves propagating parallel to the Earth's rotation axis and low velocities in the equatorial plane.

Tomographic models represent an instantaneous, low-resolution image of a convecting system. They require for their detailed interpretation knowledge of mineral and rock properties that are, as yet, poorly known but that laboratory experiments can potentially determine. The fact that the present distribution of seismic anomalies must represent the current configuration of thermal and compositional heterogeneity advected by mantle flow, imposes a complex set of constraints on the possible modes of convection in the mantle of which the implications have not yet been worked out; this will require numerical modelling of convection in three dimensions, which only recently has become feasible. Thus the interpretation of the 'geographical' information from seismology in terms of geodynamical processes is a matter of considerable complexity, and we may expect that a number of the conclusions to be drawn from the seismological results lie in the future.

Introduction

Plate tectonics, which, over the past 20 years, has provided the framework for understanding large-scale geological processes, describes the motion of large, rigid sections of the Earth's crust and uppermost mantle. The plates are transported by mantle convection currents, but a definitive understanding of mantle convection has not yet been reached. Seismic tomography offers the opportunity to investigate the interior of the convective system by mapping, in three dimensions, the seismic wave velocity variations. These are related to temperature and

---

Note on plates 1 and 2. The maps shown in these plates are labelled with the following keys: *Depth*: in kilometres; *parameter*: v_P = P-velocity; v_S = S-velocity; CMB = core-mantle boundary topography; *Div* = plate velocity divergence; *data type*: *T* = arrival-time data; *W* = waveform data; *M* = normal mode data. In plate 2 the scale at the bottom of each panel applies to each of the plates above it. In the case of v_P the range of the scale is that given by the upper pair of labels on the scale (±0.5% or ±0.3%), and in the case of v_S the range is given by the lower pair of labels (±1.0% or ±0.6%).

Description of plate 1

Plate 1. (*a*, *b*, *c*, *d*) Three-dimensional sections of models M84C and L02.56, together with a schematic illustration of the anisotropic properties of the inner core. The depth of the section, in kilometres, is indicated. In the upper-mantle panels (550 km) the depth scale is exaggerated by a factor of 5. Plate boundaries (yellow) are indicated. (*e*) Relative S-velocity perturbations in the model U84L85/SH at the depth of 150 km, characteristic of the uppermost mantle. Plate boundaries are indicated. (*f*) The truncated spherical harmonic expansion, to degree 8, of the horizontal divergence of the instantaneous plate velocity field (Minster & Jordan 1978; Forte & Peltier 1987). Units are 10^{-9} a^{-1}. (*g*) The plate divergence field, spherical harmonic degrees 2 and 3 only. See caption to (*f*). (*h*) An upper-mantle section through the S-velocity model U84L85/SH, taken along the great circle passing horizontally through the centre of the accompanying map; depth, running vertically, is in the interval 22 km–670 km; vertical exaggeration is 20:1. (*i*) Topography of the core–mantle boundary from the study of Morelli & Dziewonski (1987*a*). Blue areas are elevated and orange areas are depressed; see scale. The model contains spherical harmonics up to degree 4. (*j*) The predicted surface divergence field (degrees 2 and 3 only) using the model U84L85/SH and the density/velocity scaling $\mathrm{d} \ln \rho / \mathrm{d} \ln v_S = 0.16$ in the upper mantle and 0.20 in the lower mantle. Upper-mantle viscosity is 10^{21} Pa s and lower mantle viscosity is 3×10^{22} Pa s. See caption to plate 1*f*, *g*.

PHILOSOPHICAL TRANSACTIONS OF THE ROYAL SOCIETY A MATHEMATICAL, PHYSICAL & ENGINEERING SCIENCES

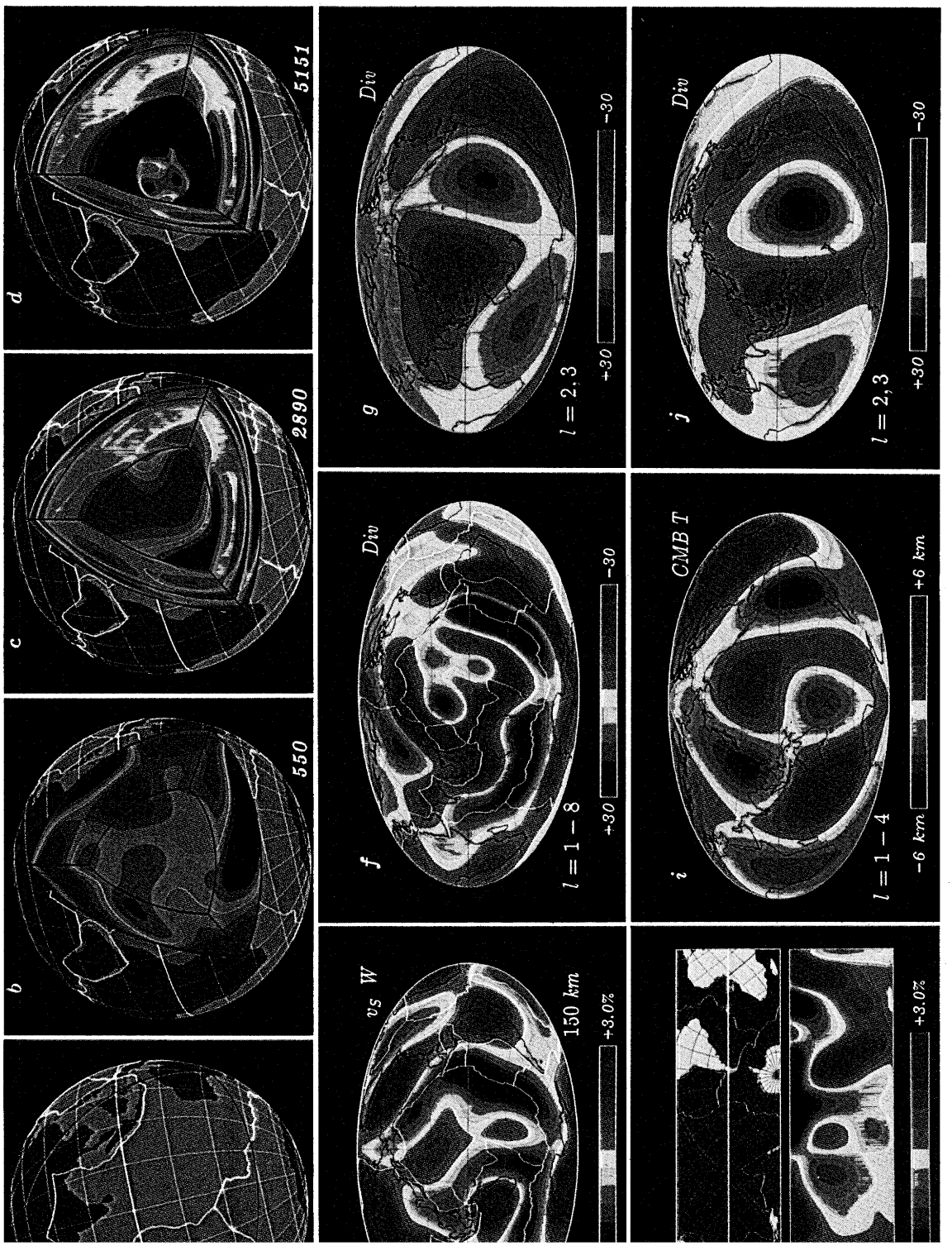

PLATE 1. For description see opposite.

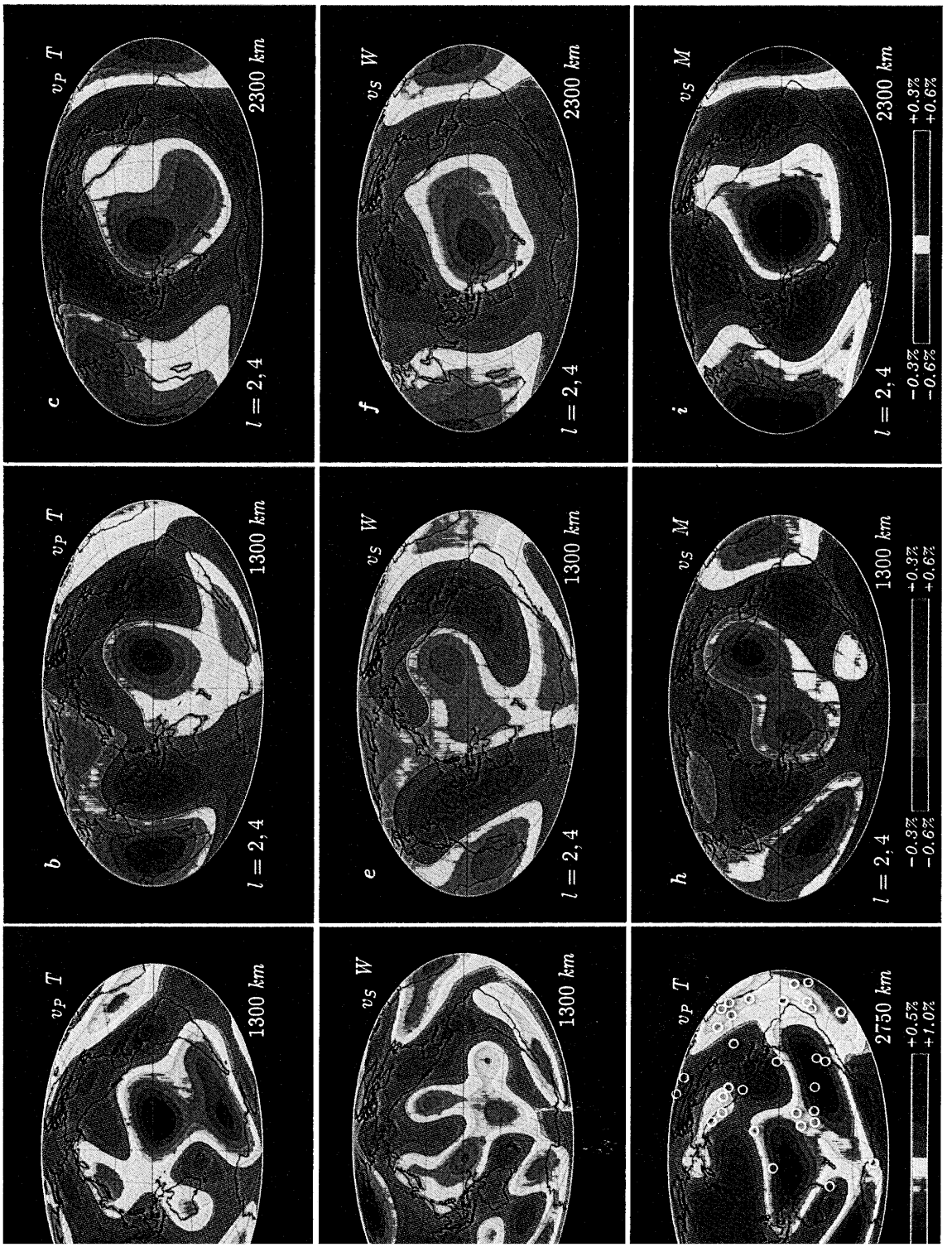

PLATE 2. For description see previous page.

composition and, in particular, to the density variations which provide the driving force of mantle convection.

Following large and intermediate earthquakes, seismic waves can be observed at stations throughout the world and significant progress has recently been made in solving the inverse problem in which very large collections of seismic data are used to reconstruct an image of the pattern of high and low wave velocities in three dimensions. Although the global images made up to now contain only the largest scale features of the Earth's three-dimensional structure, some of the conclusions to be drawn from this new 'geographical' information are now emerging. By virtue of improvements in global coverage by seismic instruments and of increasingly powerful analysis and computational techniques, there is the prospect of more detailed images in the future. In this article we discuss a number of techniques that have been applied to the global tomographic inverse problem and the models that they have lead to.

Plate 1*a*, *b*, *c*, *d* shows a composite of models of the upper-mantle S-velocity (M84C: Woodhouse & Dziewonski 1984) and the lower-mantle P-velocity (L02.56: Dziewonski 1984), and a schematic representation of the anisotropic properties of the inner core (Woodhouse *et al.* 1986; Morelli *et al.* 1986). The colour scale is such that red colours indicate lower than average wave velocities at a given depth and blue indicates higher than average velocities. These figures illustrate the scale lengths of global heterogeneity that have been resolved. In the upper mantle, the model is expanded up to degree 8 in spherical harmonics and as a cubic polynomial in depth, corresponding to nominal resolving lengths of roughly 2500 km horizontally and 150 km vertically. In the lower mantle the model is expanded up to degree 6 and as a quartic polynomial in depth, corresponding to resolving lengths of roughly 3000 km and 400 km respectively. These models represent, therefore, the result of a spatial filter applied to the true state of heterogeneity in the Earth. Such filtered versions of reality would, perhaps, be of limited interest if heterogeneity on smaller scales were dominant, but it appears that the spatial spectrum of heterogeneity contains very strong long wavelength components. In the upper mantle, for instance, S-velocity variations in spherical harmonic degrees up to 5 are as large as $\pm 4\%$ in the upper 150 km and are much larger than the expected signature of subducted slabs in this range of wavelengths. Similarly in lower-mantle P-velocity spherical harmonic degrees 2 and, to a lesser extent, 4 are dominant terms and have amplitudes of the order $\pm 0.5\%$ (plate 2*c*).

The study of lateral heterogeneity is of great significance to seismology. For example, in the investigation of earthquakes lateral heterogeneity like an imperfect lens, can distort the image of an event. Estimates of location, fault length, and the pattern of stress release can be false if the medium is inadequately known. Even the introduction of corrections for long wavelength

Description of plate 2

Plate 2. (*a*) The P-velocity travel-time model V3.I of Morelli & Dziewonski (1986) at depth 1300 km. The model contains spherical harmonics up to degree 6. (*b*) Model V3.I, depth 1300 km, degrees 2 and 4 only; see caption to (*a*). (*c*) Model V3.I, depth 2300 km, degrees 2 and 4 only; see caption to (*a*). (*d*) The S-velocity model U84L85/SH of Woodhouse & Dziewonski (1986) at depth 1300 km. The model contains spherical harmonics up to degree 8. (*e*) Model U84L85/SH, depth 1300 km, degrees 2 and 4 only; see caption to (*d*). (*f*) Model U84L85/SH, depth 2300 km, degrees 2 and 4 only; see caption to Plate (*d*). (*g*) Model V3.I, depth 2750 km (the base of the mantle), all degrees 1–6; hot spots are indicated; see caption to (*a*). (*h*) 'Model 1' of Giardini *et al.* (1987), S-velocity from free oscillation data, spherical harmonic degrees 2 and 4 only, depth 1300 km. (*i*) 'Model 1', depth 2300 km; see caption to (*h*).

PHILOSOPHICAL TRANSACTIONS OF THE ROYAL SOCIETY A MATHEMATICAL, PHYSICAL & ENGINEERING SCIENCES

lateral heterogeneity can result in shifts in inferred epicentres by as much as 20 km and changes in origin times of more than 1 s.

Outside the field of seismology, the recent results on the Earth's three dimensional structure have an impact on other fields of Earth sciences. Several examples of such linkage follow.

Mantle convection

Under the assumption that seismic anomalies are proportional to density perturbations, they provide constraints on the modelling of mantle convection and on the viscosity distribution in the mantle (Richards & Hager 1984; Forte & Peltier 1987, 1989; Hager & Clayton 1989).

Petrology and geochemistry

Models of seismic anomalies in the upper mantle show the oceanic ridges to be the dominant regions of low velocity at shallow depth. The long-wavelength models discussed in this article have the potential to provide integral constraints on petrological and thermal models of the ridge systems. Deep high-velocity anomalies are associated with the continental shields, apparently confirming the hypothesis of 'continental roots' (Jordan 1975, 1978*a*). About 80% of hot spots occur over regions of lower than average wave velocities near the core–mantle boundary (see plate 2*g*). There also appears to be a correlation between a band of low-velocity anomalies near the core–mantle boundary, in the latitude band from 10° S to 30° S, and the occurrence of a large-scale isotopic anomaly (Dupal anomaly: Hart 1984; Castillo 1988).

Geomagnetism

The regions at the core–mantle boundary where the magnetic field changes with time most rapidly coincide with low-velocity seismic anomalies, which, presumably, represent regions of elevated temperature in the lowermost mantle. The inference has been made that the thermal state of the lowermost mantle determines the stability of convection patterns, and hence of the geomagnetic field, in the outer core (Bloxham & Gubbins 1987).

Gravity

It was early recognized (Dziewonski *et al.* 1977) that there was a strong correlation between P-velocity anomalies in the lower mantle and the long-wavelength geoid undulations, but that the correlation had the opposite sign from that expected if high velocities correspond to high densities as would be the case if temperature fluctuations were responsible for the seismically observed anomalies. It has been shown, however (Pekeris 1935; Richards & Hager 1984; Hager *et al.* 1985), that density anomalies embedded in a fluid mantle induce deflections of the free surface and of the core–mantle boundary, which can change the sign of the inferred geoid perturbations; thus lower-mantle heterogeneity has been identified as a major cause of long-wavelength geoid anomalies.

Mineral physics

An example of an *in situ* measurement made possible through seismic tomography is the ratio of relative perturbations in the shear and compressional velocities: $\mathrm{d} \ln v_S / \mathrm{d} \ln v_P$. The tomographic results yield a ratio much higher than determined, at relatively low pressures, in the laboratory (Anderson *et al.* 1968). It appears that under the temperature and pressure conditions appropriate for the lower mantle, the shear modulus is much more sensitive to

PHILOSOPHICAL TRANSACTIONS OF THE ROYAL SOCIETY A MATHEMATICAL, PHYSICAL & ENGINEERING SCIENCES

changes in temperature than the bulk modulus. Similar observations for the upper mantle have been interpreted as being associated with partial melting (Hales & Doyle 1967).

Geodesy and astronomy

From the analysis of data on the Earth's rotation, obtained by the VLBI (very long-baseline interferometry) technique, it has been determined that the flattening of the Earth's core departs from its equilibrium value by 400 ± 100 m (Gwinn *et al.* 1986). Although the seismically determined core mantle boundary topography (Morelli & Dziewonski 1987*a*; plate 1*i*) has a range of ± 6 km, the component corresponding to excess flattening is very small, and error estimates are such that the seismic results are consistent with the geodetically determined flattening.

Studies of the large-scale three-dimensional structure of the Earth have been carried out using various kinds of seismological data, spanning more than three orders of magnitude in frequency (1 Hz–0.0005 Hz). These are (i) large collections of P (and PKP, PKIKP, PcP) travel times, (ii) measurements of phase and group delays and amplitude anomalies of surface waves and measurements of the locations of spectral peaks of fundamental modes, interpreted asymptotically, (iii) complete waveforms of mantle waves, used as data in a least-squares inversion, (iv) complete waveforms of long-period body waves and (v) complete spectra of split multiplets in the Earth's free oscillation spectrum. A recent review is by Dziewonski & Woodhouse (1987).

Studies of class (i) have illuminated lower-mantle P-velocity structure (Dziewonski *et al.* 1977; Dziewonski 1984; R. W. Clayton & R. Comer, unpublished) and those of classes (ii) and (iii) have led to models of upper-mantle S-velocity (Masters *et al.* 1982; Nakanishi & Anderson 1982, 1983, 1984; Woodhouse & Dziewonski 1984; Nataf *et al.* 1984, 1986). With the addition of classes (iv) and (v) (Woodhouse & Dziewonski 1986; Tanimoto 1987; Giardini *et al.* 1987, 1988) it has become possible to constrain lower-mantle S-velocity structure and thus to obtain models of the same region of the Earth by using different classes of data. This is very valuable in that it provides a check on the various modelling techniques and also allows the comparison of heterogeneity in different structural parameters in the same region. With one kind of data alone, it is often difficult to completely rule out the possibility that systematic errors or deficiencies in coverage, which are inherent in the data, degrade or corrupt the resulting models. We find, however, that the application of different techniques is yielding a coherent picture of the Earth's global heterogeneity, reinforcing the conclusions drawn from each data set alone.

In §2 below we outline the general framework of the tomographic inverse problem and in §3 we discuss some of the techniques that have been employed and intercompare the resulting models.

2. The tomographic inverse problem

Observations of seismic disturbances contain information about the earthquakes that generate them – for instance the location and origin time of the event, the orientation of faulting and so forth – and about the structure of the Earth. The mechanics of the Earth's linear, adiabatic, elastic vibrations, which describes all seismic motions except those in the immediate vicinity of an earthquake, is characterized, in the case of an isotropic material, by

PHILOSOPHICAL TRANSACTIONS OF THE ROYAL SOCIETY A MATHEMATICAL, PHYSICAL & ENGINEERING SCIENCES

the bulk modulus $\kappa(\boldsymbol{x})$, the shear modulus $\mu(\boldsymbol{x})$ and the density $\rho(\boldsymbol{x})$, where $\boldsymbol{x}$ is position. At relatively high frequencies (larger than 0.2 Hz, say) wave propagation is well described in terms of packets of energy propagating along optical rays. In the solid portions of the Earth there exist compressional waves (P-waves) having velocity $v_P = [(\kappa + \frac{4}{3}\mu)/\rho]^{\frac{1}{2}}$ and shear waves (S-waves) of velocity $v_S = [\mu/\rho]^{\frac{1}{2}}$; in the fluid outer core and the ocean μ and v_S vanish and shear waves do not exist. For an anisotropic material a number of other moduli must be introduced and the wave velocities depend upon the local direction of travel and on the polarization of the wave, but these are complications that we shall neglect in this article.

To clarify the discussion of the tomographic inverse problem we here outline a simple but general formalism that encompasses all of the specific applications to be considered later. Let d_n^s represent the nth observation relating to the sth earthquake source. Data d_n^s may represent, for example, the arrival time of a particular seismic phase at the nth receiver, or it may represent the nth sample in a large array of waveforms or spectra from a number of stations. In general, d_n^s will be functionals of observed seismograms and will be very numerous. Let f_k^s denote the necessary source parameters relating to the sth source; for arrival time data f_i^s $(i = 1,2,3,4)$ will consist of the location and origin time of the event and for waveform or spectral data they will also include parameters describing the size of the event and the geometry of faulting. Given a model of the Earth $\boldsymbol{E} = [v_P(\boldsymbol{x}), v_S(\boldsymbol{x}), \rho(\boldsymbol{x})]$ we may, in principle, predict the expected values of the observations:

$$d_n^s = D_n[\boldsymbol{f}^s, \boldsymbol{E}] + \epsilon_n^s, \tag{1}$$

where D_n is a known function of $\boldsymbol{f}^s$ and functional of $\boldsymbol{E}(\boldsymbol{x})$ and ϵ_n^s is observational error. In practical applications it is necessary to represent the continuous function $\boldsymbol{E}(\boldsymbol{x})$ in terms of a finite set of parameters. We shall write

$$\boldsymbol{E}(\boldsymbol{x}) = \boldsymbol{E}_0(r) + \sum_{klm} E_{klm}\, \boldsymbol{m}_{klm}(\boldsymbol{x}), \tag{2}$$

where r is radius, $\boldsymbol{E}_0(r)$ is a spherically symmetric, reference earth model and $\boldsymbol{m}_{klm}(\boldsymbol{x})$ are a chosen set of basis functions depending upon three indices k, l, m. It is possible, for example, to partition the Earth into a three-dimensional array of cells labelled by a radial index, k, a latitude index, l and a longitude index m and to define $\boldsymbol{m}_{klm}(\boldsymbol{x})$ to be $[1,0,0]$ in the (k,l,m)th cell and to vanish elsewhere; in this case the expansion coefficient E_{klm} would represent the deviation of P-velocity in the (k,l,m)th cell from that of the reference model. This approach has been used in both regional and global studies (see, for example, Aki *et al.* 1977; Dziewonski *et al.* 1977). Another approach, which we have employed in the studies described below, is to choose $\boldsymbol{m}_{klm}(x)$ to consist of certain smooth functions, e.g.

$$\boldsymbol{m}_{klm}(\boldsymbol{x}) = \boldsymbol{m}_k(r)\, Y_l^m(\theta, \phi), \tag{3}$$

where (r, θ, ϕ) are spherical coordinates (radius, colatitude, longitude), $Y_l^m(\theta, \phi)$ are spherical harmonics and where $\boldsymbol{m}_k(r)$ $(k = 1,2,\ldots,K)$ are a set of (orthogonal) radial vector functions. In this case, E_{klm} represent the expansion coefficients in a spherical harmonic series, also expanded in radius.

By using any expansion of the form (2), equation (1) may be written

$$d_n^s = D_n[\boldsymbol{f}^s, \boldsymbol{E}_0 + \sum_{klm} E_{klm}\, \boldsymbol{m}_{klm}(\boldsymbol{x})] + \epsilon_n^s. \tag{4}$$

The tomographic inverse problem may be thought of as that of characterizing the set of solutions (f_i^s, E_{klm}) consistent with assumed statistical properties of the errors and with statistical *prior information* on the model parameters (see Tarantola & Valette 1982*a*). If the corresponding distributions are assumed to be gaussian then (4) leads to a version of the least-squares technique. If the covariances $\mathrm{cov}(\epsilon_n^s, \epsilon_{n'}^{s'})$ are specified it is, in principle, straightforward to linearly transform the data in such a way that the transformed errors are independent gaussian variates of uniform variance σ^2, say. Similarly a linear transformation of the set of unknowns (f_i^s, E_{klm}) may be found such that the prior information consists of requiring that the transformed unknowns be independent samples of a gaussian distribution of variance η^2, say. In the interests of being concise we shall here assume that the data and model parameters in (4) already possess these simple statistical properties and that there is no prior information on source parameters. In this case the maximum likelihood estimate of the unknowns (f_i^s, E_{klm}), the expectation of the *a posteriori* distribution, is that which minimizes

$$L \equiv \sigma^{-2} \sum_{ns} \{d_n^s - D_n[f^s, E_0 + \sum_{klm} E_{klm} m_{klm}(x)]\}^2 + \eta^{-2} \sum_{klm} \{E_{klm} - E_{klm}^0\}^2, \tag{5}$$

where E_{klm}^0 is a prior heterogeneous model (the expectation of the *a priori* distribution of model parameters, usually zero in applications). This has the form

$$L = \sigma^{-2}|\boldsymbol{d} - \boldsymbol{D}(\boldsymbol{x}, \boldsymbol{y})|^2 + \eta^{-2}|\boldsymbol{x} - \boldsymbol{x}^0|^2, \tag{6}$$

where the algebraic vectors $\boldsymbol{d}, \boldsymbol{x}, \boldsymbol{y}$ correspond to the data, the model parameters and the source parameters for all sources, respectively.

Because, in general, $\boldsymbol{D}(\boldsymbol{x}, \boldsymbol{y})$ is a nonlinear function of its arguments, the minimization of (6) is an iterative process (Tarantola & Valette 1982*a*, *b*) in which the partial derivatives of $\boldsymbol{D}(\boldsymbol{x}, \boldsymbol{y})$ are required. For travel-time data these are provided by Fermat's principle, by which the travel-time increment corresponding to a perturbation in wave speed may be calculated in terms of an integral along the unperturbed ray path; in general, the partial derivatives must be obtained through a theoretical analysis of the wave propagation problem and will be given by a form of the Born approximation. It is of interest to note that whereas the accuracy of these derivatives will influence the rate of convergence to a minimum, it will not affect the value $(\boldsymbol{x}_\infty, \boldsymbol{y}_\infty)$ say, to which, let us assume, the iterates converge. Assuming convergence, the accuracy of the solution minimizing (6) depends only upon that with which it is possible to calculate the solution of the forward problem, $\boldsymbol{D}(\boldsymbol{x}, \boldsymbol{y})$.

This formalism also allows the estimation of the *a posteriori* statistics of $(\boldsymbol{x}, \boldsymbol{y})$ provided that it is sufficient to represent $\boldsymbol{D}(\boldsymbol{x}, \boldsymbol{y})$ by a linear approximation in the neighbourhood of $(\boldsymbol{x}_\infty, \boldsymbol{y}_\infty)$.

In the event that no prior information or insufficient prior information is available, the solution minimizing (6) may be indeterminate. In this case an important concept is that of *resolution* (Backus & Gilbert 1968; Jackson 1979; Gubbins & Bloxham 1985). Recognizing that the minimization of (6) does not yield a useful estimate of $\boldsymbol{x}$, one seeks a transformation

$$\boldsymbol{x}' = \boldsymbol{R}\boldsymbol{x} \tag{7}$$

such that $\boldsymbol{x}'$ has suitably small *a posteriori* errors. The operator $\boldsymbol{R}$, which ideally is close to the identity, represents linear combinations of model parameters which are estimable within a chosen level of error. This operator is commonly chosen to coincide with that which results

PHILOSOPHICAL TRANSACTIONS OF THE ROYAL SOCIETY A MATHEMATICAL, PHYSICAL & ENGINEERING SCIENCES

from the incorporation of fictitious *prior information*, although it is possible to define other strategies for choosing $\boldsymbol{R}$ to achieve desired resolution and error characteristics in the solution. The quality of a solution $\boldsymbol{x}'$ is then characterized by its errors (more generally by its covariance matrix) and its resolution operator $\boldsymbol{R}$. The concept of resolution does not easily generalize to nonlinear problems, and thus one needs to perform such analysis in the neighbourhood of $(\boldsymbol{x}_\infty, \boldsymbol{y}_\infty)$ using a linearized approximation to $\boldsymbol{D}(\boldsymbol{x}, \boldsymbol{y})$; in this case the results of such calculations must be interpreted with caution, because they do not correctly represent the statistical estimation problem.

The usefulness of the formalism outlined here is limited by our inability, in most cases, to realistically characterize the statistical properties of the errors ϵ_n^s. Far from being independent gaussian samples there are invariably many potential sources of systematic error which are essentially impossible to discover or to quantify. An example would be the potential biasing effect on tomographic models caused by the fact that seismic sources preferentially occur in or near subduction zones, the locations of which are highly correlated with larger-scale patterns of mantle heterogeneity.

The 'errors' in (1) also include components that are not properly described as observational errors. In the case that complete seismograms are used as data, the function D_n in (1) consists of an algorithm for the calculation of synthetic seismograms, and although at long periods it is possible, in principle, to calculate accurate synthetic seismograms, such calculations are too laborious to be feasible in application to the inversion of large data sets. Thus applications of this technique have used asymptotic (ray theoretic) approximations to the effects of heterogeneity which undoubtedly are often subject to appreciable theoretical errors.

Probably the largest source of discrepancy between data and model predictions arises from unmodelled structure, which is not describable in terms of the chosen set of basis functions $\boldsymbol{m}_{klm}(\boldsymbol{x})$. An example is the potential effects due to anisotropy on a model that does not contain anisotropic parameters. The answer to such difficulties is not always to include more model parameters, because in this case many of them may become impossible to usefully constrain. In a linear problem it is possible to calculate which linear combinations of model parameters can be estimated with a given level of error, but the usefulness of this is questionable; new scientific conclusions are unlikely to result from knowing the values of a number of linear combinations of disparate model parameters, which are, however, insufficient to give estimates of any individual one. The information contained in a given data set, if all potential model parameters are included, consists of a statistical distribution in a model space of high dimension; but such a distribution is impossible to visualize and thus it is impossible to make any useful inference.

Instead, in our view, one must proceed on the basis of certain hypotheses: for example, the hypothesis that errors in synthetic seismogram techniques do not vitiate inversion results, or the hypothesis that the effects of mantle anisotropy do not corrupt the results of an inversion for isotropic structure. There arise opportunities to test such hypotheses when it proves to be possible to investigate the same region of the Earth using different kinds of data and different modelling techniques. For example, a very-long-wavelength, high-velocity structure in the lower mantle, bearing a clear relationship to the locations of subduction zones (see below), has been independently found using P-wave arrival times, vertically polarized long-period P–SV waveforms, horizontally polarized SH waveforms and spectra of free oscillations. These data sets are fundamentally different in their sensitivities to unmodelled effects, and different

PHILOSOPHICAL TRANSACTIONS OF THE ROYAL SOCIETY A MATHEMATICAL, PHYSICAL & ENGINEERING SCIENCES

theoretical techniques are used in each case. Low-degree free oscillations, for example, are insensitive to the locations of sources; vertically and horizontally polarized shear waves have greatly different sensitivities to anisotropy and different from that of P-waves; the waveform data consist largely of multiple reflections of S-waves by the free surface and therefore their sensitivity to mantle structure differs greatly from that of the direct P-wave; in addition they are much less sensitive to near-surface effects. By the intercomparison of models built by using different techniques it is possible to test the validity of the approximations or simplifying assumptions which, out of necessity, have been made.

The above statements of caution regarding the estimation of errors and resolution are not peculiar to the tomographic problem. In the determination of the hypocentral location of earthquakes, for example, formal error analysis invariably underestimate true uncertainties, for the same reasons as discussed above. Even if the Earth were perfectly spherically symmetric, the fact that measures of uncertainty have not been determined for spherically symmetric models of the Earth would make it impossible to correctly quantify the uncertainty in hypocentral locations. These problems are greatly compounded by the presence of lateral heterogeneity and anisotropy. We discuss this issue in the context of tomographic modelling because in the studies discussed here the models are formally overdetermined to such an extent that the conventional error estimates, scaling inversely as the square root of the number of data, give unrealistically small estimates of uncertainty. What is usually meant by an error estimate is actually a measure of the sensitivity of the solution to statistical fluctuations in the data. In the tomographic problems outlined in this article this is small, and is only a minor component of the true uncertainty as measured, for example, by independent inversions from different partitions of a given data set (see, for example, Woodhouse & Dziewonski 1984) or by the intercomparison of models constructed with different kinds of data. It is our aim in this discussion simply to note that in attempting to quantify the uncertainties in tomographic models, conventional formulae based upon the above statistical formalism, are usually inadequate, owing to the failure of the 'errors' in the data to satisfy the underlying statistical assumptions.

3. Tomographic techniques and models

The foregoing analysis identifies aspects that the particular techniques, to be discussed here, have in common. A technique is characterized by specifying (i) the data set, (ii) the theoretical algorithm $D_n[\boldsymbol{f}^s, \boldsymbol{E}]$, (iii) the basis functions $\boldsymbol{m}_{klm}(\boldsymbol{x})$ and (iv) the statistical assumptions concerning the distribution of 'errors' and the choice of resolution operator. Naturally, if modelling results are greatly sensitive to the somewhat arbitrary choices that enter into this formulation, the results are called into question. Here we discuss several specific techniques and present some comparisons of corresponding models.

3.1. *Arrival times*

Arrival times of the principal seismic phases are read by station operators around the world and are reported to the International Seismological Centre (ISC), which publishes them both in its printed bulletin and in computer-readable form. These voluminous catalogues, containing readings from more than 1000 stations, have proved to be a valuable resource in determining both the spherical and the aspherical structure of the Earth. The seismic phases from which such readings are made have a characteristic period of approximately 1 s.

Analysis of the arrival times of the direct P-wave have led to models of lower-mantle P-velocity (Dziewonski *et al.* 1977; Dziewonski 1984; Morelli & Dziewonski 1986). The data set assembled by Morelli & Dziewonski (1986), for example, consists of approximately 1.7×10^6 selected readings, relating to some 26000 events. In selecting and reducing the data, steps are taken to desensitize the solution to the potential effects of crustal structure beneath the stations and to the effects of subducted slabs (see Dziewonski 1984; Morelli & Dziewonski 1987*b*). The theoretical technique used in this problem is that given by geometrical ray theory, linearized by means of Fermat's principle, and the basis functions correspond to a spherical harmonic expansion of P-velocity up to degree 6 and a radial representation as a quartic polynomial in the depth range corresponding to the lower mantle.

Some of the properties of the model V3.I of Morelli & Dziewonski (1986), which are shared by the similar model L02.56 of Dziewonski (1984), are illustrated in plate 2*a*, *b*, *c*, *g*. Plates 2*a* and 2*g* are maps at the depths 1300 km and 2700 km, which are representative of the top and the bottom of the lower mantle, respectively. Plates 2*b* and 2*c* show the components of the model in spherical harmonic degrees 2 and 4 at depths 1300 and 2300 km. The pattern of high velocities encircling the Pacific, largely contained in degrees 2 and 4, is a dominant feature of such models and the pattern of plate 2*c* (2300 km depth) is relatively constant over a large range of depths, changing appreciably only within a few hundred kilometres of the top and the bottom of the lower mantle. Plate 2*g* shows the distribution of hot spots superimposed on the model at the base of the lower mantle, suggesting an association between the locations of hot spots with regions of low P-velocity in the lowermost mantle.

3.2. *Seismic waveforms*

Starting in the mid-1970s, the Global Digital Seismograph Network (GDSN), operated by the United States Geological Survey, and the International Deployment of Accelerometers (IDA) network, operated by the University of California, San Diego, have provided continuous, digital, long-period seismic data from a global array of receivers. During the 1980s the French GEOSCOPE network has furnished additional three-component long-period data. The digital recordings from these networks have made it possible, for the first time, to assemble very large waveform data bases for use in seismic inversion.

Theoretical studies of the free oscillations of an aspherical Earth (see Dahlen 1968) and the development of an asymptotic formalism for the interpretation of frequency shifts due to heterogeneity (Jordan 1978*b*; Silver & Jordan 1981) led to the discovery of a strong degree 2 pattern in the phase-velocity variations of fundamental-mode Rayleigh waves having periods longer than about 220 s (Masters *et al.* 1982), which was identified as originating in the transition zone (400–650 km depth).

Employing somewhat higher frequencies and using a technique capable of resolving odd-degree heterogeneity as well as even degrees and of incorporating overtone data in addition to the fundamental mode branch, Woodhouse & Dziewonski (1984) constructed a three-dimensional model of upper-mantle S-velocity containing degrees up to 8 and represented as a cubic polynomial in depth. The technique developed for this study is based upon least-squares fitting of entire waveforms of very long period ($f < \frac{1}{135}$ Hz) 'mantle waves', world-circling Rayleigh and Love waves sensitive principally to upper-mantle structure. An example of such data, together with synthetic seismograms for three models, is shown in figure 1. The principal information in this kind of data is contained in mismatches in phase between data and

PHILOSOPHICAL TRANSACTIONS OF THE ROYAL SOCIETY A MATHEMATICAL, PHYSICAL & ENGINEERING SCIENCES

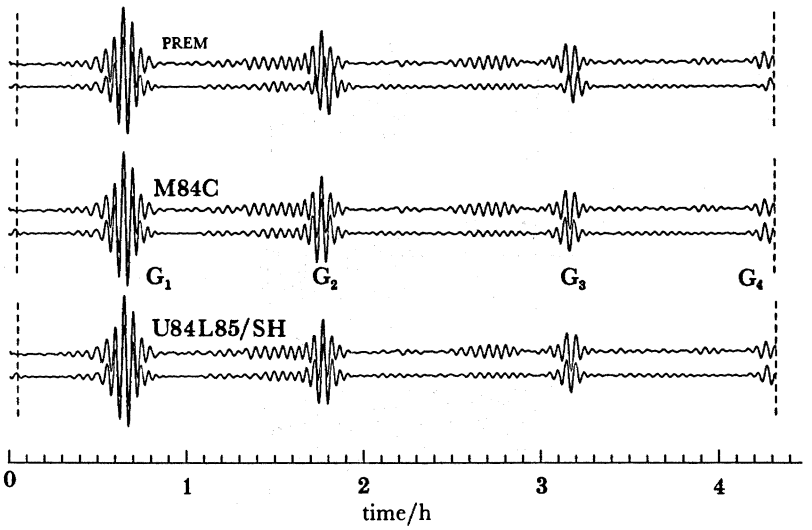

FIGURE 1. An example of very-long-period 'mantle wave' data used in the waveform inversion study discussed in the text. The data are from the station NWAO (Western Australia) of the Global Digital Seismographic Network, following an event on the Mid-Atlantic Ridge on 3 June 1981; epicentral distance is 99.5°. In each pair of traces the top trace is the data, low-pass filtered by using a cut-off frequency $\frac{1}{135}$ Hz and the bottom trace is a theoretical seismogram for a particular Earth model. The two observed horizontal components of motion have been combined to yield the transverse component. The large arrivals are the world-circling Love waves G_1, G_2 etc. In the top pair of traces the synthetic seismogram is calculated for the spherically symmetric model PREM of Dziewonski & Anderson (1981); large phase errors are evident in the major group arrivals. In the middle pair of traces (model M84C; Woodhouse & Dziewonski 1984) these phase misalignments have been largely eliminated, and similarly in the bottom pair, which corresponds to the model based upon SH waves discussed in the text. Note that the model U84L85/SH matches wave data approximately to the same degree as the model M84C, which is based upon mantle wave data alone; U84L85/SH also includes information from body waves such as those shown in figure 2.

theoretical seismograms, which are representative of certain averages along the source–receiver path and with depth of the three-dimensional variations in v_S (mainly) and v_P. The modelling strategy succeeds in greatly reducing such discrepancies, for a large suite of data, by adjusting the three dimensional distribution of variations in v_S.

More recently another kind of data consisting of long-period body waves ($f \leqslant \frac{1}{45}$ Hz) together with a larger set of mantle wave data have been used to construct global models of v_S for both the upper and the lower mantle (Woodhouse & Dziewonski 1986). Examples of the body-wave data are shown in figure 2. The largest arrivals in such data are multiple reflections of S-waves from the free surface. Woodhouse & Dziewonski (1986; the definitive versions of these models are in preparation) have used a data set consisting of some 6600 mantle wave records and 8500 body wave records from 220 globally distributed events. Analysis has been performed separately on the horizontally polarized (SH) and vertically polarized (P–SV) subsets of the data, to assess the potential effects of anisotropy; here we shall discuss only the results for SH; the SH model is designated U84L85/SH.

The theoretical technique used in these studies is based upon an asymptotic approximation to the effects of heterogeneity (Woodhouse & Dziewonski 1984; Mochizuki 1986; Romanowicz 1987), which has as one of its advantages the property that a theoretical seismogram corresponding to a given source–receiver pair depends only upon the horizontally averaged structure along the great circle path between the source and receiver. It is this property that makes feasible the calculation of large numbers of partial derivative seismograms because, for

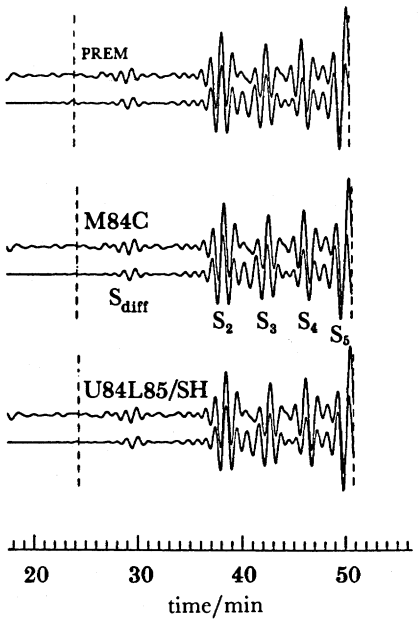

FIGURE 2. An example of long-period body-wave data; the data are the transverse component from the station KONO (Norway) following an event in the Western Pacific on 15 February 1982; epicentral distance is 123.1°. As in figure 1 the observed seismogram is the top trace of each pair, in this case low-pass filtered with a cut-off frequency $\frac{1}{45}$ Hz. The phase labelled S_{diff} is the S-wave diffracted by the core; S_n ($n = 2,3,4,5$) are the phases SS, SSS, etc., which have suffered $n-1$ reflections from the free surface between the source and the receiver. Phase errors evident in the top two pairs are greatly reduced by the model U84L85/SH, discussed in the text. See caption to figure 1.

a given source–receiver pair, it is only those linear combinations of the model parameters corresponding to the path-averaged structure that enter into the calculation. The accuracy of this approximation for fundamental modes has been investigated by Park (1987) who finds that it represents well the largest effects of heterogeneity. Further tests of this approximation and the development of more accurate techniques are certainly desirable.

The model derived by this approach from SH data is shown in plates 1*e*, *h* and 2*d*. In common with earlier models, large low-velocity anomalies are associated with mid-oceanic ridges, which, moreover, are strongest for the most rapidly spreading ridges (East-Pacific Rise, Southeast Indian Rise) and weaker for less active ridges (Mid-Atlantic Ridge). This is evident in plate 1*e*, *f* in which the shear velocity distribution at 150 km depth – characteristic of the uppermost mantle – is compared with the truncated spherical harmonic expansion of the horizontal divergence of the plate velocity field (Minster & Jordan 1978). Low-velocity anomalies are also associated with the back-arc regions of the west Pacific. In addition there are large deep high-velocity anomalies beneath the continents (Jordan 1975). Notable in their apparent absence are the traces of subduction zones; although large localized anomalies are known to be associated with subducted slabs they do not have a large signature when filtered to wavelengths greater than 2000 km, which are the horizontal scale lengths of the model here described. If a slab is represented by a 10% velocity anomaly 100 km wide, its filtered representation at a wavelength of 2000 km will correspond only to a 0.5% anomaly. The anomalies corresponding to ridges and continents, on the other hand, are several percent in amplitude and thus are large enough to mask the signal corresponding to the slabs. Plate 1*h* shows a section of the upper-mantle model taken along the great circle indicated in the map;

this displays examples of the deep extensions of the continental shields and of the occurrence of low-velocity anomalies associated with ridges.

In the lower mantle this model of S-velocity is highly correlated with P-velocity models based upon travel-time data, and also with models of v_P and v_S inferred from spectral splitting of free oscillations, discussed below; the three data sets, however, require an unexpectedly large ratio of v_P and v_S anomalies, $\mathrm{d} \ln v_S / \mathrm{d} \ln v_P \approx 2$–2.5, which corresponds roughly to the case in which variations in shear modulus dominate those in bulk modulus. A thermodynamic explanation of this has been suggested by Anderson (1987). Three comparisons of the P-velocity model V3.I with the S-velocity model U84L85/SH are shown in plates 2*a*, *d*, 2*b*, *e* and 2*c*, *f*; note that the contour intervals and the range of the colour scales for relative perturbations in v_S are twice those for v_P.

The top of the lower mantle reveals high-velocity anomalies following the subduction zones of the present and the geologically recent past (see plate 2*a*, *d*). These high-velocity features include the rim of the Pacific and a region stretching roughly from Indonesia to the Mediterranean that marks the Tethys convergence zone. In plates 2*a*, *d* and 1*f*, independent models of SH-velocity and P-velocity inferred from travel times may be compared with the present-day plate divergence field. It will be noted that the anomalies are displaced outwards from the Pacific relative to the current loci of subduction, and that regions such as North America and southern Eurasia, which have been stronger convergence zones in the past than they are at present, are strongly represented in the models. In North and Central America these models are in good agreement with the regional model of Grand (1987), which shows, with somewhat higher resolution, a high-velocity, N–S trending anomaly in the depth range 800–1200 km. At its southern end, in the Carribbean, this coincides with an anomaly identified by Jordan & Lynn (1974) and by Lay (1983). Jordan & Lynn (1974) and Grand (1987) have suggested that the anomaly represents material subducted beneath the North American continent, and the fact that it forms a part of a global feature skirting most of the subduction zones of the Pacific (plate 2*a*, *d*) tends to substantiate this.

This pattern blends, with increasing depth, into long-wavelength pattern of high velocities around the Pacific that continues to the core–mantle boundary. Plate 2*c*, *f* shows the degree 2 and 4 components of this pattern at the depth 2300 km.

3.3. *Free oscillations*

Individual arrival times used in constructing tomographic models are sensitive to very-short-wavelength features of Earth structure, because typical wavelengths of 1 Hz signals are less than 10 km. To determine large-scale structure one has to rely upon an inversion algorithm to correctly evaluate the appropriate averages. Similarly the typical wavelengths of the mantle wave and long-period body wave data used in waveform inversion are significantly less than the scale lengths of the resulting models. The very low-frequency signals of free oscillations, however, having wavelengths comparable to the Earth's radius, provide the opportunity to make use of information that is directly sensitive only to the longest wavelength features of Earth structure. An isolated mode of angular order 2, for example, is sensitive only to degrees 2 and 4 in the spherical harmonic expansion of the Earth's heterogeneity. This kind of data is also unique in the sense that source and receiver bias may be essentially ruled out as a potential source of systematic error.

For modes that are 'isolated' in the spectrum, i.e. that do not exchange energy with other

PHILOSOPHICAL TRANSACTIONS OF THE ROYAL SOCIETY A MATHEMATICAL, PHYSICAL & ENGINEERING SCIENCES

modes, the theory of degenerate splitting (Dahlen 1968; Woodhouse & Dahlen 1978; Woodhouse & Girnius 1982) may be used to calculate the time series, and hence the spectrum, of the model multiplet in an aspherical Earth model; no ray theoretic approximations are needed. The splitting due to heterogeneity is quantified in terms of the *splitting function* (Woodhouse & Giardini 1985; Giardini *et al.* 1987, 1988; Woodhouse *et al.* 1986), which is analogous to a phase velocity distribution for the mode. A similar approach has been employed by Ritzwoller *et al.* (1986, 1988).

Figure 3 shows an example of observed and theoretical spectra used in such a study (Giardini *et al.* 1988). In each frame the phase spectrum in the interval $[-\pi, \pi]$ is shown in the top panel, the amplitude spectrum in the middle panel; broken lines are theoretical spectra for a given Earth model and solid lines are observed spectra. This particular spectral window (1.21–1.27 mHz) contains the two modal multiplets ${}_0S_7$, with 15 singlets, and ${}_2S_3$ with 7 singlets†. The relative amplitudes and spectral locations of the singlets contributing to the theoretical spectra are indicated in the bottom panel of each frame. The top pair of frames (figure 3*a*, *b*) show data from two different stations and theoretical spectra for a model which is elliptical and is rotating

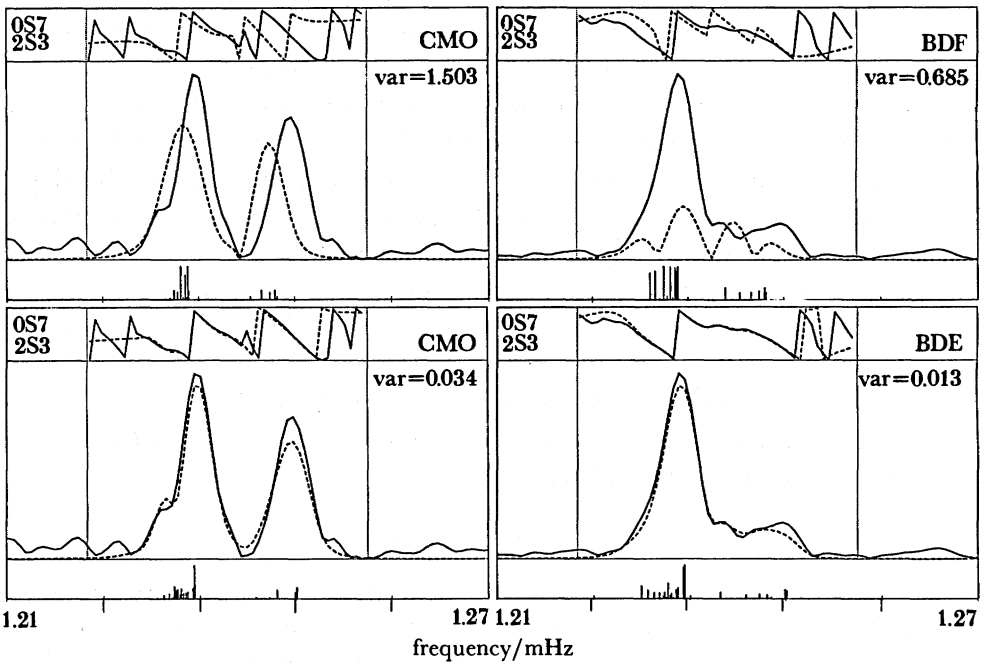

FIGURE 3. Examples of free oscillation amplitude and phase spectra from the IDA stations CMO (Alaska) and BDF (Brazil) following an event in Sumbawa, Indonesia on 19 August 1977. The top two frames show the comparison of data (solid line) with theoretical spectra (broken line) for a spherically symmetrical model, including the effects of rotation and ellipticity only. The bottom two frames show the comparison after inversion for the *splitting function* using a total of 59 spectra relating to the same pair of multiplets. The values 'var' are measures of misfit (squared misfit/squared data) in the complex spectra domain. Further details are given in the text.

† The theory of modal splitting is analogous to that describing a spherically symmetric atom subject an aspherical perturbing influence, such as a magnetic field. A degenerate multiplet ${}_nS_l$ of angular order l (c.f. total angular momentum) consists of $2l+1$ singlets belonging to the same eigenfrequency (c.f. energy level) and labelled by their azimuthal order numbers $-l, -l+1, \ldots, l-1, l$ (c.f. z-components of angular momentum). An aspherical pertubation leads to $2l+1$ eigenfunctions belonging to distinct eigenfrequencies, which, to zeroth order, are various linear combinations of the $2l+1$ degenerate eigenfunctions.

but is otherwise spherically symmetric. It will be noted that the differences between data and synthetics are very large in both amplitude and in phase. Observed spectra do not allow one to resolve individual singlets owing to the effects of attenuation and finite record length; the observed peaks are broad and represent the combined effects of the interference of the contributing singlets. The lower frames (figure 3*c*, *d*) show the same data, together with theoretical spectra after inversion for the *splitting functions* of these two multiplets. It should be noted that the data shown are but two records from a total of 59 records, from 10 events, which were used in this inversion. Thus our inability to resolve the fine structure in the spectra of individual records is compensated by the requirement that all available data in this spectral window, corresponding to different source–station pairs, must be explained simultaneously by the same distribution of singlets, having excitation amplitudes consistent with independently determined source parameters. The problem is further constrained by requiring the splitting to be due only to heterogeneity of degrees 2 and 4. Thus the problem is, at least formally, greatly overdetermined; the variance ratios (squared misfit/squared data) before and after inversion for all 59 traces are 0.689 and 0.134, respectively, in this case.

Modes sensitive primarily to mantle S-velocity structure have been used to obtain models of the lower mantle (Giardini *et al.* 1987), albeit of limited resolution (spherical harmonic degrees 2 and 4); these show strong correlation with travel-time models of v_P and, when compared quantitatively with these models, give a high value of $\mathrm{d} \ln v_S / \mathrm{d} \ln v_P \approx 2$–2.5, in agreement with conclusions drawn from the waveform models discussed above. Some mantle models also have non-negligible sensitivity to v_P, and provide evidence that the level of v_P heterogeneity is the same at modal periods (300–2100 s) as it is found to be at 1 s period in travel-time studies (Giardini *et al.* 1987, 1988). Modal models of v_S, at depths 1300 km and 2300 km are shown in plate 2*h*, *i* (Giardini *et al.* 1987). The two right-hand panels in plate 2 show three independent determinations of lower-mantle heterogeneity of degrees 2 and 4. The pattern of high velocities around the Pacific, largely contained in degree 2, has thus been independently obtained from three different kinds of data.

4. Discussion

From studies such as those discussed above, some of the major features of the Earth's three-dimensional structure are becoming clear and the process of interpretation is underway. In the upper mantle the continental shields are characterized by deep (*ca.* 300 km) high-velocity anomalies (see Jordan 1978*a*; Woodhouse & Dziewonski 1984) and the strongest low-velocity features are associated with the fast-spreading oceanic ridges (plate 1*e*, *h*, *g*). Whereas the latter can be understood in terms of the upwelling of hot material as the plates move apart, the deep extensions of the continents present some difficulty because it may be expected that vigorous convection would rapidly destroy them. Probably they are compositionally different, cooler and of higher viscosity than the sub-oceanic mantle (Jordan 1988). By translating the observed velocity anomalies into density anomalies and performing a dynamical calculation of fluid flow in a mantle of assumed viscosity structure, these models have been used to infer the expected fluid motion at the surface (Forte & Peltier 1987). Comparison with the poloidal component of the observed motion of the plates shows fairly good agreement at very low degree (plate 1*g*, *j*), and highly significant correlations at higher degrees and thus it has become possible to begin to understand the internal forces that drive plate motion. A limiting factor,

PHILOSOPHICAL TRANSACTIONS OF THE ROYAL SOCIETY A MATHEMATICAL, PHYSICAL & ENGINEERING SCIENCES

however, is the unknown relation between density and velocity variations beneath the continents; conventional assumptions lead to difficulty in explaining surface topography and the geoid.

Much interest in geodynamics centres on the trajectory in the mantle of material subducted at convergent plate boundaries. This is because it bears on the question of how well the mantle is mixed, which is of great importance in understanding the Earth's chemical evolution. Although the debate on this issue will doubtless continue for some time to come, the most natural inference from both global (Dziewonski 1984; Woodhouse & Diezwonski 1986) and regional (see Creager & Jordan 1984, 1986; Grand 1987) seismological studies is that cold subducted material penetrates the boundary, although a significant increase in viscosity may act to reduce the velocity and to increase the cross-sectional area of the descending flow (Hager *et al.* 1985). Present day subduction takes place principally around the rim of the Pacific; models of the lower mantle show that a very-long-wavelength pattern of high velocities around the Pacific (see plate 2) persists throughout the lower mantle (Dziewonski *et al.* 1977; Dziewonski 1984; Woodhouse & Dziewonski 1986; Morelli & Dziewonski 1986; Giardini *et al.* 1987) and, moreover, that its morphology bears the closest resemblence to what may be expected due to subduction in the upper part of the lower mantle (plate 2*a*, *d*). This feature, which fills a major fraction of the Earth's volume, is undoubtedly of fundamental significance in understanding the Earth's long-term dynamics; it remains to be determined, through geodynamical modelling, whether this feature *explains* or whether it is *explained by* the fact that subduction zones have tended to be in fixed locations for long periods of Earth history. That is: is the tomographically observed anomaly to be attributed to material subducted in the same locations for long periods of time, or are the locations of convergent plate boundaries governed by a long-lived thermal anomaly in the lower mantle? Just outside the core the pattern of high and low velocities is such that approximately 80% of hot spots at the surface are above regions of lower than average velocity in the lowermost mantle, lending support to the hypothesis that hot spots are the surface manifestation of plumes rooted in the deepest part of the mantle (plate 2*g*). Instantaneous fluid dynamical calculations have had major success in explaining the very long wavelength geoid perturbations as the result of density anomalies, proportional to the seismic velocity anomalies in the lower mantle, acting as internal loads in a viscous mantle and have led to the conclusion that the viscosity of the lower mantle is substantially higher than that of the upper mantle (Hager *et al.* 1985).

The shape of the core–mantle boundary, in spherical harmonic degrees up to 4, has been determined by using the travel times of both reflected and transmitted waves (Morelli & Dziewonski 1987*a*), yielding consistent results where coverage is adequate (plate 1*i*). Fluid dynamical calculations have again been successful in explaining some aspects of the seismically inferred boundary topography (Forte & Peltier 1989). However, studies incorporating rays that have high angles of incidence (almost grazing) have shown a different pattern (Creager & Jordan 1987). This apparent discrepancy is probably a further manifestation of the complex heterogeneity in the lowermost mantle and, possibly, in the outermost core. It is important to recognize that a deflection in the core–mantle boundary produces an anomaly in the travel time of a reflected phase (PcP) that has the opposite sign from the travel-time anomaly of the transmitted wave (PKP) which intersects the boundary at the same point. A velocity anomaly in the mantle, on the other hand, would produce travel-time anomalies of the same sign in PcP and PKP. In the study of Morelli & Dziewonski (1987*a*), the demonstration that PcP gives a

PHILOSOPHICAL TRANSACTIONS OF THE ROYAL SOCIETY A MATHEMATICAL, PHYSICAL & ENGINEERING SCIENCES

result similar to that obtained from PKP (and, in particular, a result of the same sign) is strong evidence that it is truly the signal of a boundary deflection, rather than that of mantle heterogeneity, that has been detected.

Although no well-documented heterogeneity has been reported in the fluid outer core – and, indeed, is not to be expected because of the inability of an inviscid fluid to maintain such heterogeneity – the inner core has been found to be characterized by an anisotropic, crystalline structure (Woodhouse *et al.* 1986; Morelli *et al.* 1986; Shearer *et al.* 1988) in which there is preferential alignment of the high velocity axes parallel to the Earth's rotation axis. This enigmatic observation is possibly evidence of low-degree convection in the inner core (Jeanloz & Wenk 1988).

We are grateful to our collaborators in much of the work reviewed in this article: D. Giardini, X.-D. Li and A. Morelli. We also thank the staff of Albuquerque Seismological Laboratory, United States Geological Survey; of the IDA Project, University of California, San Diego; and of the International Seismological Centre. These dedicated laboratories have provided the data used in the studies reported upon here. The work has been supported by the following grants from the United States National Science Foundation: EAR83-17594, EAR86-18829, EAR87-08622, EAR87-21301.

References

Aki, K., Christofferson, A. & Husebye, E. S. 1977 *J. geophys. Res.* **82**, 277–296.
Anderson, D. L. 1987 *Physics Earth planet. Inter.* **45**, 307–323.
Anderson, O. L., Schreiber, E., Liebermann, R. C. & Soga, M. 1968 *Rev. Geophys.* **6**, 491–524.
Backus, G. E. & Gilbert, J. F. 1968 *Geophys. Jl R. astr. Soc.* **16**, 169–205.
Bloxham, J. & Gubbins, D. 1987 *Nature, Lond.* **325**, 511–513.
Castillo, P. R. 1988 *Eos, Wash.* **69**, 490, 491.
Creager, K. C. & Jordan, T. H. 1984 *J. geophys. Res.* **89**, 3031–3049.
Creager, K. C. & Jordan, T. H. 1986 *J. geophys. Res.* **91**, 3573–3589.
Creager, K. C. & Jordan, T. H. 1987 *Eos, Wash.* **68**, 1487.
Dahlen, F. A. 1968 *Geophys. Jl R. astr. Soc.* **16**, 329–367.
Dziewonski, A. M. 1984 *J. geophys. Res.* **89**, 5929–5952.
Dziewonski, A. M. & Anderson, D. L. 1981 *Physics Earth planet. Inter.* **25**, 297–356.
Dziewonski, A. M. & Woodhouse, J. H. 1987 *Science, Wash.* **236**, 37–48.
Dziewonski, A. M., Hager, B. H. & O'Connell, R. J. 1977 *J. geophys. Res.* **82**, 239–255.
Forte, A. M. & Peltier, W. R. 1987 *J. geophys. Res.* **92**, 3645–3679.
Forte, A. M. & Peltier, W. R. 1989 *Tectonophysics.* (In the press.)
Giardini, D., Li, X.-D. & Woodhouse, J. H. 1987 *Nature, Lond.* **325**, 405–411.
Giardini, D., Li, X.-D. & Woodhouse, J. H. 1988 *J. geophys. Res.* **93**, 13716–13742.
Grand, S. P. 1987 *J. geophys. Res.* **92**, 14065–14090.
Gubbins, D. & Bloxham, J. 1985 *Geophys. Jl. R. astr. Soc.* **80**, 695–713.
Gwinn, C. R., Herring, T. A. & Shapiro, I. I. 1986 *J. geophys. Res.* **91**, 4755–4765.
Hager, B. H. & Clayton, R. W. 1989 In *Mantle convection* (ed. W. R. Peltier). New York: Gordon & Breach. (In the press.)
Hager, B. H., Clayton, R. W., Richards, M. A., Comer, R. P. & Dziewonski, A. M. 1985 *Nature, Lond.* **313**, 541–545.
Hales, A. L. & Doyle, H. A. 1967 *Geophys. Jl R. astr. Soc.* **13**, 403–415.
Hart, S. R. 1984 *Nature, Lond.* **309**, 753–757.
Jackson, D. D. 1979 *Geophys. Jl R. astr.* **57**, 137–157.
Jeanloz, R. & Wenk, H.-R. 1988 *Geophys. Res. Lett.* **15**, 72–75.
Jordan, T. H. 1975 *Rev. Geophys. Space Phys.* **13**, 1–12.
Jordan, T. H. 1978*a* *Nature, Lond.* **274**, 544–548.
Jordan, T. H. 1978*b* *Geophys. Jl R. astr. Soc.* **52**, 441–455.
Jordan, T. H. 1988 *J. Petr.* Special lithosphere issue, pp. 11–37.
Jordan, T. H. & Lynn, W. S. 1974 *J. geophys. Res.* **79**, 2679–2685.

PHILOSOPHICAL TRANSACTIONS OF THE ROYAL SOCIETY A MATHEMATICAL, PHYSICAL & ENGINEERING SCIENCES

Lay, T. 1983 *Geophys. Jl R. astr. Soc.* **72**, 483–516.
Masters, G., Jordan, T. H., Silver, P. G. & Gilbert, F. 1982 *Nature, Lond.* **298**, 609–613.
Minster, J. B. & Jordan, T. H. 1978 *J. geophys. Res.* **83**, 5331–5354.
Mochizuki, E. 1986 *Geophys. Res. Lett.* **13**, 1478–1481.
Morelli, A. & Dziewonski, A. 1986 *Eos, Wash.* **67**, 311.
Morelli, A. & Dziewonski, A. M. 1987*a* *Nature, Lond.* **325**, 678–683.
Morelli, A. & Dziewonski, A. M. 1987*b* In *Seismic tomography* (ed. G. Nolet), pp. 251–274. D. Reidel.
Morelli, A., Dziewonski, A. M. & Woodhouse, J. H. 1986 *Geophys. Res. Lett.* **13**, 1545–1548.
Nakanishi, I. & Anderson, D. L. 1982 *Bull. Am. seism. Soc.* **72**, 1185–1194.
Nakanishi, I. & Anderson, D. L. 1983 *J. geophys. Res.* **88**, 10267–10283.
Nakanishi, I. & Anderson, D. L. 1984 *Geophys. Jl R. astr. Soc.* **78**, 573–618.
Nataf, H.-C., Nakanishi, I. & Anderson, D. L. 1984 *Geophys. Res. Lett.* **11**, 109–112.
Nataf, H.-C., Nakanishi, I. & Anderson, D. L. 1986 *J. geophys. Res.* **91**, 7261–7307.
Park, J. 1987 *Geophys. Jl R. astr. Soc.* **90**, 129–169.
Pekeris, C. L. 1935 *Mon. Not. R. astr. Soc. geophys. Suppl.* **3**, 343–367.
Richards, M. A. & Hager, B. H. 1984 *J. geophys. Res.* **89**, 5987–6002.
Ritzwoller, M., Masters, G. & Gilbert, F. 1986 *J. geophys. Res.* **91**, 10203–10228.
Ritzwoller, M., Masters, G. & Gilbert, F. 1988 *J. geophys. Res.* **93**, 6369–6396.
Romanowicz, B. 1987 *Geophys. Jl R. astr. Soc.* **90**, 75–100.
Shearer, P. M., Toy, K. & Orcutt, J. A. 1988 *Nature, Lond.* **333**, 228–232.
Silver, P. G. & Jordan, T. H. 1981 *Geophys. Jl R. astr. Soc.* **64**, 605–634.
Tanimoto, T. 1987 *Eos, Wash.* **68**, 1487, 1488.
Tarantola, A. & Valette, B. 1982*a* *J. Geophys.* **50**, 159–170.
Tarantola, A. & Valette, B. 1982*b* *Rev. Geophys. Space Phys.* **20**, 219–232.
Woodhouse, J. H. & Dahlen, F. A. 1978 *Geophys. Jl R. astr. Soc.* **53**, 335–354.
Woodhouse, J. H. & Dziewonski, A. M. 1984 *J. geophys. Res.* **89**, 5953–5986.
Woodhouse, J. H. & Dziewonski, A. M. 1986 *Eos, Wash.* **67**, 307.
Woodhouse, J. H. & Giardini, D. 1985 *Eos, Wash.* **66**, 300.
Woodhouse, J. H. & Girnius, T. P. 1982 *Geophys. Jl R. astr. Soc.* **68**, 653–673.
Woodhouse, J. H., Giardini, D. & Li, X.-D. 1986 *Geophys. Res. Lett.* **13**, 1549–1552.

PHILOSOPHICAL TRANSACTIONS OF THE ROYAL SOCIETY A MATHEMATICAL, PHYSICAL & ENGINEERING SCIENCES

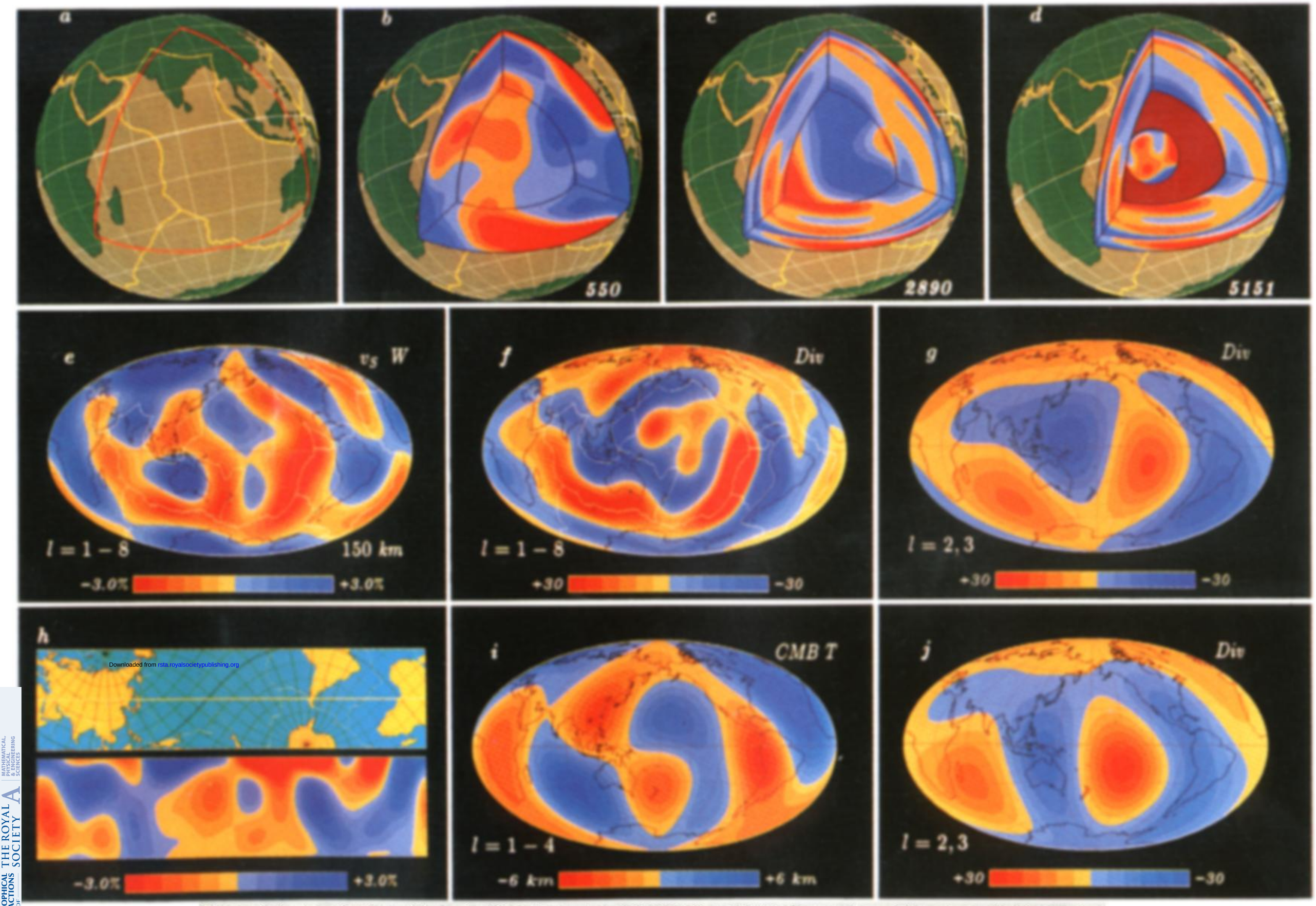

PHILOSOPHICAL TRANSACTIONS OF THE ROYAL SOCIETY A MATHEMATICAL, PHYSICAL & ENGINEERING SCIENCES

PLATE 1. (*a*, *b*, *c*, *d*) Three-dimensional sections of models M84C and L02.56, together with a schematic illustration of the anisotropic properties of the inner core. The depth of the section, in kilometres, is indicated. In the upper-mantle panels (550 km) the depth scale is exaggerated by a factor of 5. Plate boundaries (yellow) are indicated. (*e*) Relative S-velocity perturbations in the model U84L85/SH at the depth of 150 km, characteristic of the uppermost mantle. Plate boundaries are indicated. (*f*) The truncated spherical harmonic expansion, to degree 8, of the horizontal divergence of the instantaneous plate velocity field (Minster & Jordan 1978; Forte & Peltier 1987). Units are 10^{-9} a^{-1}. (*g*) The plate divergence field, spherical harmonic degrees 2 and 3 only. See caption to (*f*). (*h*) An upper-mantle section through the S-velocity model U84L85/SH, taken along the great circle passing horizontally through the centre of the accompanying map; depth, running vertically, is in the interval 22 km–670 km; vertical exaggeration is 20:1. (*i*) Topography of the core–mantle boundary from the study of Morelli & Dziewonski (1987*a*). Blue areas are elevated and orange areas are depressed; see scale. The model contains spherical harmonics up to degree 4. (*j*) The predicted surface divergence field (degrees 2 and 3 only) using the model U84L85/SH and the density/velocity scaling $\mathrm{d} \ln \rho / \mathrm{d} \ln v_s = 0.16$ in the upper mantle and 0.20 in the lower mantle. Upper-mantle viscosity is 10^{21} Pa s and lower mantle viscosity is 3×10^{22} Pa s. See caption to plate 1*f*, *g*.

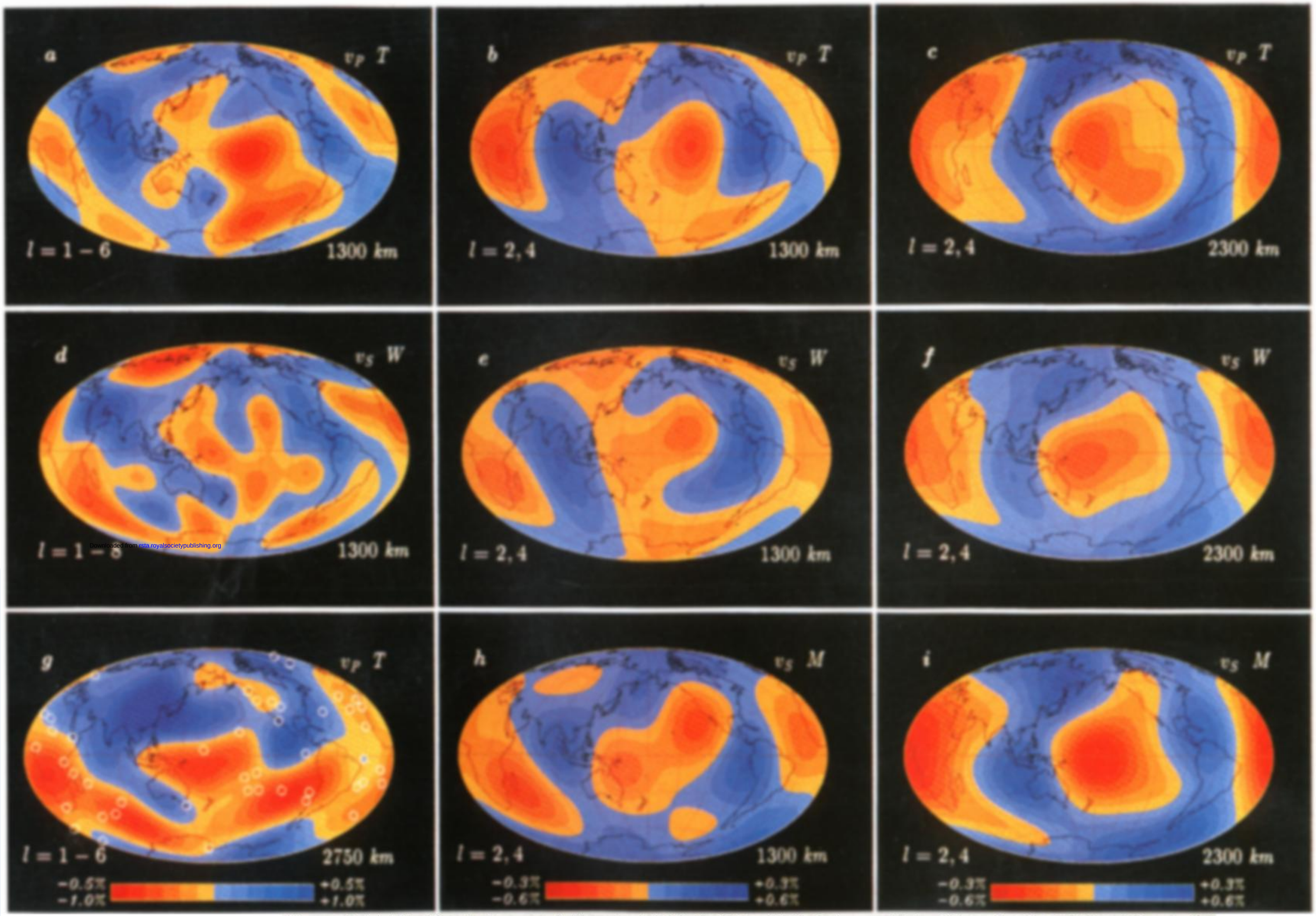

PLATE 2. (*a*) The P-velocity travel-time model V3.I of Morelli & Dziewonski (1986) at depth 1300 km. The model contains spherical harmonics up to degree 6. (*b*) Model V3.I, depth 1300 km, degrees 2 and 4 only; see caption to (*a*). (*c*) Model V3.I, depth 2300 km, degrees 2 and 4 only; see caption to (*a*). (*d*) The S-velocity model U84L85/SH of Woodhouse & Dziewonski (1986) at depth 1300 km. The model contains spherical harmonics up to degree 8. (*e*) Model U84L85/SH, depth 1300 km, degrees 2 and 4 only; see caption to (*d*). (*f*) Model U84L85/SH, depth 2300 km, degrees 2 and 4 only; see caption to Plate (*d*). (*g*) Model V3.I, depth 2750 km (the base of the mantle), all degrees 1–6; hot spots are indicated; see caption to (*a*). (*h*) 'Model 1' of Giardini *et al.* (1987), S-velocity from free oscillation data, spherical harmonic degrees 2 and 4 only, depth 1300 km. (*i*) 'Model 1', depth 2300 km; see caption to (*h*).

PHILOSOPHICAL TRANSACTIONS OF THE ROYAL SOCIETY A MATHEMATICAL, PHYSICAL & ENGINEERING SCIENCES